Research Square

Preprints are preliminary reports that have not undergone peer review.
They should not be considered conclusive, used to inform clinical practice,
or referenced by the media as validated information.

6-Hydroxydopamine Induce Neurodegeneration In Terminally Differentiated SH-SY5Y Neuroblastoma Cells Via Enrichment Of The Nucleosomal Degradation Pathway: A Global Proteomic Approach

Kasthuri Bai Magalingam
International Medical University
Sushela Devi Somanath
International Medical University
Premdass Ramdas
International Medical University
Nagaraja Haleagrahara
James Cook University
Ammu Kutty Radhakrishnan (ammu.radhakrishnan@monash.edu)
Monash University Malaysia https://orcid.org/0000-0003-2638-907X

Research Article

Keywords: Parkinson's disease (PD), 6-hydroxydopamine (6-OHDA), human neuroblastoma cells (SH-SY5Y)

Posted Date: April 30th, 2021

DOI: https://doi.org/10.21203/rs.3.rs-441687/v1

License: This work is licensed under a Creative Commons Attribution 4.0 International License.
Read Full License

Version of Record: A version of this preprint was published at Journal of Molecular Neuroscience on March 8th, 2022. See the published version at https://doi.org/10.1007/s12031-021-01962-z.

Abstract

The SH-SY5Y human neuroblastoma cells have been used for decades as an *in vitro* cell model of dopaminergic neurons to explore the underlying science of cellular and molecular mechanisms of neurodegeneration in Parkinson's disease (PD). However, data revealing the protein expression changes in 6-OHDA induced cytotoxicity in differentiated SH-SY5Y cells remain void. Therefore, we investigated the differentially regulated proteins expressed in terminally differentiated SH-SY5Y cells (differ-SH-SY5Y neural cells) exposed to 6-hydroxydopamine (6-OHDA) using the LC-MS/MS technology and interpreted the data using the online bioinformatics databases such as PANTHER, STRING, and KEGG. Our studies demonstrated the neuronal development in differ-SH-SY5Y neural cells was implicated by the overexpression of proteins responsible for neurite formations such as calnexin (CANX) and calreticulin (CALR) besides significant down-regulation of ribosomal proteins. The enrichment of the KEGG ribosome pathway was detected with significant down-regulation ($p < 0.05$) of all the 21 ribosomal proteins in differ-SH-SY5Y neural cells compared with undifferentiated cells. Whereas in the PD model, the pathological changes induced by 6-OHDA were indicated by the presence of unfolded and misfolded proteins, which triggered the response of 10 kDa heat shock proteins, namely HSPE1 and HSPA9. Moreover, the 6-OHDA induced neurodegeneration in differ-SH-SY5Y neural cells also upregulated the voltage-dependent anion-selective channel protein 1 (VDAC1) protein and enriched the KEGG systemic lupus erythematosus pathway that was regulated by all 17 histone proteins ($p < 0.05$) in differ-SH-SY5Y neural cells. These results suggest the central event in the neurodegenerative mechanism induced by 6-OHDA in the PD cell model was the nucleosomal degradation in the KEGG-SLE pathway indicated by the increased histone release in the apoptotic cells.

Introduction

Over the last 20 years, a significant amount of data has emerged suggesting different cellular models that are valuable in evaluating potential drug targets in modulating the disease course in Parkinson's disease. Undeniably, the immortalized SH-SY5Y human neuroblastoma cell lines have been an excellent choice for preliminary drug screening for PD. The SH-SY5Y cell line demonstrates a moderate activity of crucial neuronal markers that usually exists in dopaminergic cells such as dopamine-β-hydroxylase (Katsuyama *et al.*, 2020), tyrosine hydroxylase (Khwanraj *et al.*, 2015), choline acetyl-transferase (Filograna *et al.*, 2015) and noradrenaline (Kovalevich and Langford, 2013). Whether undifferentiated or differentiated SH-SY5Y neuroblastoma should be used as a substitute to dopamine neurons in PD-related study remains controversial. However, most neuroscience researchers have suggested that it is highly crucial to utilize differentiated SH-SY5Y human neuroblastoma cells that resemble human dopamine neurons for PD studies (Magalingam et al. 2020).

A fantastic wealth of information has been accumulated on different techniques and protocols to develop terminally matured dopamine neurons. Cheung *et al.* have pointed out that retinoic acid (RA) induced differentiation of SH-SY5Y cells demonstrated extensive outgrowth of neurite and augmentation of neuronal markers such as neuronal nuclei, enolase, synaptophysin and synaptic-associated protein-97

(Cheung *et al.*, 2009). Studies have also shown that RA-induced differentiation exhibits a low proliferative rate and increased expression of genes related to synaptic vesicle cycle, dopamine synthesis/ degradation and dopamine transporter (DAT) (Lopes *et al.*, 2017), as well as higher tyrosine hydroxylase, which is the critical enzyme in the synthesis of dopamine neurotransmitter (Khwanraj *et al.*, 2015). Furthermore, our previous studies have delineated that the RA-induced differentiation on SH-SY5Y cells in a low-serum culture medium demonstrated enhanced neurite projection with longer varicosities connecting the adjacent cells, reduced proliferation rate as well as increased levels of dopamine and alpha-synuclein. Moreover, the differentiated cell line also expresses dopaminergic characteristics at the genetic level by upregulating the DRD2 gene expression (Magalingam et al., 2020). Our findings correlate with numerous previous studies that suggested that differentiated SH-SY5Y cell line possesses the closest resemblance with dopaminergic cells and is suitable for neurodegenerative related studies (Khwanraj *et al.*, 2015) (Lopes *et al.*, 2017).

Although there is ample evidence on various approaches to establishing differentiated neuronal cells, data on the 6-OHDA induced cytotoxicity on differentiated SH-SY5Y cells remains scarce. Lopes *et al.* (Lopes *et al.*, 2017) and Cheung *et al.* (Cheung *et al.*, 2009) have shown that 6-OHDA have varied susceptibility on RA-differentiated SH-SY5Y cells. Other studies have documented the biochemical changes induced by 6-OHDA on undifferentiated SH-SY5Y cells. These studies have shown that 6-OHDA-induced cytotoxicity is mediated by mitochondrial fragmentation (Gomez-Lazaro *et al.*, 2008), autophagy (Arsikin *et al.*, 2012), mitochondrial respiration (Iglesias-González *et al.*, 2012), generation of free radicals (Storch *et al.*, 2000) and changes in lipid classes (Xicoy *et al.*, 2020). Since there is no data available on the proteomic changes implicated by 6-OHDA on differentiated SH-SY5Y cells, our findings contribute to filling the knowledge gap on the molecular, biological and pathways regulated by the 6-OHDA on RA-differentiated SH-SY5Y neuroblastoma cells.

The proteomic study is an emerging field of large-scale protein expression study that provides an unprecedented insight into the cellular structural and functional framework. Intrinsically, proteins within the cell play a crucial role in providing cellular structure, movement and communication, and participates in metabolism, respiration, signal transduction and reproduction activities (Aslam *et al.*, 2017). The differential expression of proteomes in cells is a signal of significant alterations in cellular activity. The Label-free liquid chromatography coupled to tandem mass spectrometry (LS-MS/MS) technology quantifies and reveals thousands of global proteins across samples from digested peptides and matched the detected peptide/protein identity using automated database searching (Sinitcyn, Rudolph and Cox, 2018). Subsequently, the Protein ANalysis THrough Evolutionary Relationships (PANTHER) (Mi *et al.*, 2019) bioinformatic database was applied to analyse the differentially regulated proteins for their functional annotation using gene ontology (GO) (Pomaznoy, Ha and Peters, 2018). The Search Tool for the Retrieval of Interacting Genes/Proteins (STRING) (Szklarczyk *et al.*, 2019) and Kyoto Encyclopaedia of Genes and Genomes (KEGG) (Kanehisa, 2019) search engines were utilized to understand the protein-protein interaction, enriched bio-pathway and molecular function.

In the present study, we performed label-free global protein profiling of terminally differentiated SH-SY5Y (differ-SH-SY5Y) neural cells and the cell model of PD using 6-hydroxydopamine-induced neurodegeneration of differ-SH-SY5Y cells based on a shotgun proteomic methodology. The main objective of this study was to identify the novel biomarkers and pathways involved in the neuronal development of SH-SY5Y cells and the cellular model of PD. The functional role and enriched canonical pathway of the differentially expressed proteins identified from these studies were further explored using bioinformatic tools. This study further authenticates the use of the 6-OHDA induced cytotoxicity on differ-SH-SY5Y cell model as an important tool in the investigation of potential drug targets for PD.

Methods

Cell culture

The SH-SY5Y neuroblastoma cells (Cat # CRL-2266) were grown in a complete culture medium containing 88% of Dulbecco Modified Eagle Medium (DMEM) supplemented with 4.5 g/L glucose and L-glutamine without sodium pyruvate (Corning, Corning, NY, U.S.A), 10% heat-inactivated fetal bovine serum (FBS, Biosera, Nuaille, France), 1% Penicillin-streptomycin (P/S) (Gibco, Carlsbad, U.S.A) and 1% non-essential amino acid (NEAA, GIBCO, Carlsbad, U.S.A) 37^{o}C in a humidified 5% CO_2 incubator. The culture medium was replaced every 3-days, and cells were sub-cultured once it reaches 70% confluence.

Differentiation of SH-SY5Y neuroblastoma cells

The establishment of differ-SH-SY5Y neural cells was performed by seeding 1 x 10^5 cells/mL of SH-SY5Y human neuroblastoma cells in a complete culture medium in a T75 flask. After 24 hours of cell seeding, the cells were exposed to a differentiation medium containing 95% of DMEM, 3% heat-activated FBS, 1% P/S, 1% NEAA and 10 µM of all trans-retinoic acid (RA, Sigma Aldrich, St. Louis, U.S.A) for 6-days. After 6-days of the differentiation phase, the differ-SH-SY5Y neural cells express dopaminergic characteristics at morphological, biochemical and genetic levels (Magalingam et al. 2020).

Preparation and Treatment protocol of 6-hydroxydopamine (6-OHDA)

6-Hydroxydopamine (6-OHDA, Sigma Aldrich, St. Louis, U.S.A) was freshly prepared using chilled 0.15% ascorbic acid (Sigma Aldrich, St. Louis, U.S.A) and sterilized by filtering through a syringe filter fitted with a 0.2 mM filter and stored in the dark at 4^{o}C to protect it from light. On day 7 (after the 6-days of differentiation phase), the differ-SH-SY5Y cells were exposed to 10 µg/mL of 6-OHDA in a serum-free culture medium for 24 hours. The undifferentiated cells were maintained in a serum-free culture medium without 6-OHDA for the same duration of time. The concentration of 6-OHDA (10 µg/mL) was selected based on the preliminary studies that showed that it inhibited proliferation of the differ-SH-SY5Y neural cells by about 50%.

Protein extraction

On day 8, the undifferentiated, differ-SH-SY5Y, and 6-OHDA exposed differ-SH-SY5Y neural cells were harvested from the T75 flasks and recovered by centrifugation *(1000 g for 10 min at 4^{o}C)*. The supernatant was discarded, and the total protein was extracted from the cells using the EasyPrep Mini MS Sample Prep kit (Thermo Fisher Scientific, U.S.A). Briefly, 100 µL of lysis buffer *(provided with the kit)* and 1 µL of universal nuclease *(provided with the kit)* were added to the cell pellets and thoroughly mixed until the sample's viscosity reduced. The extracted protein samples were aliquoted and stored at -80°C until further use.

Determination of protein concentration

The extracted proteins' concentration was estimated using the Pierce BCA Protein Kit (Thermo Fisher Scientific, U.S.A) (El-Rami et al. 2017). The absorbance was measured at 562 nm using a microplate reader (SpectramaxM, CA, USA). A standard curve was prepared by plotting the average corrected absorbance measurements of BSA standards vs concentration in µg/mL to determine the 'unknown samples' protein concentrations.

Protein reduction and alkylation

The extracted proteins were subjected to reduction and alkylation steps followed by protein digestion and a "clean-up" procedure using the EasyPrep Mini MS Sample Prep kit protocol. The samples were removed from the -80°C freezer and thawed at room temperature. Once samples were liquefied, 100 µg of protein from each sample was transferred into appropriately labelled sterile 1.5 mL tubes, and the final volume for each sample was adjusted to 100 µL with lysis solution *(provided with the kit)*. Then, 50 µL of reduction solution *(provided with the kit)* was added to each tube and mixed gently. Following this, 50 µL of alkylation solution *(provided with the kit)* was added to the tubes, and the tubes were gently mixed. The tubes were incubated at 95°C using a heat block for 10 minutes to reduce and alkylation reactions. Following this, the samples were removed from the heat block to cool to room temperature and subjected to Trypsin/Lys-C protein digestion procedure.

Trypsin/Lys-C protein digestion

For the digestion step, 500 µL of the enzyme reconstitution solution *(provided with the kit)* was added to a vial containing Trypsin/Lys-C-Protease mix *(provided with the kit)*. Then, 50 µL of the reconstituted Trypsin/Lys-C-Protease mix was added to each tube containing the samples, and the tubes were incubated at 37°C with shaking for 3 hours to allow protein digestion to take place. At the end of 3 hours, 50 µL of digestion stop solution *(provided with the kit)* was added to each tube to terminate the digestion process.

Peptide clean-up

After the peptide digestion, any contaminants present in the samples were sequentially removed using the peptide clean-up column *(provided with the kit)*. The peptide clean-up columns were labelled

accordingly to avoid any sample mix-ups. As per the manufacturer recommended protocol, the white cap at the bottom of each peptide clean-up column was removed, and its green top cap loosened before each clean-up column was placed in individual 2 mL tubes. The tubes were centrifuged *(3000 g for 2 minutes)* to remove trapped liquid from the column, and the flow-through from each column was discarded. The digested peptides from each sample were transferred into the respective peptide clean-up column. The columns were centrifuged *(1500 g for 2 minutes)*, and the flow-through from each column was discarded. Next, wash solution A *(provided with the kit)* was added into each column before centrifugation, and the flow-through from each column was discarded. This step was repeated using wash solution B *(provided with the kit)*. Before the elution step, the peptide columns were centrifuged to remove any residual fluid. Then, each column was placed on appropriately labelled sterile collection tubes, and elution solution *(provided with the kit)* was added to each column. The eluted peptide samples were collected by centrifugation, dried using a vacuum centrifuge and stored at -80°C before LC-MS/MS analysis.

Liquid Chromatography and Mass Spectrometry Analysis

The digested peptides were loaded into an Agilent 1200 HPLC-Chip/MS Interface, coupled with Agilent 6550 iFunnel Q-TOF LC/MS (Agilent, Santa Clara, CA, USA). The column was equilibrated with 0.1% formic acid in water (solution A). The peptides were eluted from the column with 90% acetonitrile in 0.1% formic acid in water (solution B). Quadrupole-time of flight (Q-TOF) polarity was set at positive with capillary and fragmenter voltage being set at 1900 V and 360 V, respectively, and 5 L/min of gas flow with a temperature of 325 ◦C. The collision energy was determined at 3.7V (100Da), and reference masses with positive polarity was set at 299.294457 and 1221.990637. The peptide spectrum was analysed in auto MS mode ranging from 110–3000 m/z for MS scan and 50–3000 m/z for MS/MS scan.

Data Computation

The raw data of tryptic peptides were extracted and processed using PEAKS X software (Bioinformatics Solutions Inc., Waterloo, ON, Canada) using Uniprot, Swissprot and TrEMBL databases. The PEAKS X software allows for the determination of the protein abundance using the following search parameters: retention time lower bound: ≥ 0, retention time upper bound: ≤ 55, average area: ≥ 0, charge lower bound: ≥ 1, confident number samples per group: ≥ 1, peptide identification count: ≥ 1, protein significance: ≥ 20, used peptides: ≥ 1, fixed modification: Carbamidomethylation of cysteine residues and false discovery rate (FDR): 1% in three biological replicate injections. Protein abundance was computed using normalized spectral protein intensity (LFQ intensity). The obtained peptide/protein list was exported to Microsoft Excel to quantitate three biological replicates from the same samples were grouped in the same matrix. The protein data were filtered for at least two valid values, and protein only presented in one biological replicate was eliminated. The biological replicates from all samples were clustered under the same matrix, and the missing data were assigned with a random number derived from a normal distribution. The reason for the missing data measurement is due to low protein abundance in LC-MS/MS analysis.

Biocomputational Protein analysis

Protein Functional classification was performed using the gene ontology database

The identified proteins with *p<0.05* against their respective control were classified based on (i) molecular function, (ii) biological process and (iii) cellular component using Gene Ontology (GO) term analysis. The online bioinformatics tool PANTHER database (http://pantherdb.org) version 16 was used to elucidate the functions of these differentially expressed proteins in the differ-SH-SY5Y neural cells and 6-OHDA exposed differ-SH-SY5Y cells. Only the top 10 enriched GO terms were listed for each functional classification. All results displayed expressed adjusted *p-value* < 0.05 as determined by Fischer's Exact test and FDR.

Protein-Protein Interaction (PPI) Analysis

The STRING database (STRINGv11.0) (https://string-db.org) was used to construct the PPI network in neuronal maturation and oxidative stress in 6-OHDA treated neural cells based on its physical binding and regulatory interaction. The Uniprot IDs of the differentially regulated proteins were inputted in the STRING database under the multiple protein analysis categories and followed by the selection of *Homo Sapiens* from organism pull-down selection. The basic settings that were used in the analysis of PPI are Network type: Full network, active interaction sources: text mining, neighbourhood, experiments, databases, co-expression, gene-fusion, co-occurrence, Minimum required interaction score: highest confidence (0.9) and K-mean clustering was specified as three clusters. Thick edges between the protein nodes demonstrate strong protein interaction. This protein cluster was uploaded into Cytoscape 3.8.0 to visualise the complex networks by integrating Log2 fold-change data.

Pathway Enrichment Analysis

The pathway enrichment analysis of the differentially expressed proteins was performed using DAVID (Database for Annotation, Visualization and Integrated Discovery, https://david.ncifcrf.gov/) bioinformatic online database. The cluster with the most enriched proteins exhibiting strong PPI identified from STRING analysis was uploaded as an official gene symbol in DAVID resources. The enriched pathway curated by KEGG (Kyoto Encyclopaedia of Genes and Genomes) was used to elucidate the differentially regulated protein molecular mechanisms.

Statistical analysis

Statistical analysis comparing the quantitative data from differential protein expression between differ-SH-SY5Y neural cells vs undifferentiated SH-SY5Y cells and 6-OHDA treated differ-SH-SY5Y neural cells vs untreated differ-SH-SY5Y cells were performed using a two-tailed Student's t-test. All statistical analyses were performed with GraphPad Prism version 9.0. Differentially expressed proteins that displayed the difference in Log2 Fold change (< or > 0) with *p<0.05* were regarded as statistically significant.

Results

Label-Free Spectrometry Identification and Quantification of differentially regulated proteins

The protein profiling of differ-SH-SY5Y neural cells vs undifferentiated SH-SY5Y cells and 6-OHDA induced neurodegeneration vs untreated differ-SH-SY5Y were analysed using PEAKS X + software. The label-free tandem liquid mass spectrometry (LC-MS/MS) identified a total of 3261 and 3873 proteins for the differentiated and undifferentiated SH-SY5Y neural cells, respectively. Around 687 and 941 proteins were common in all the biological triplicates in differ-SH-SY5Y and undifferentiated SH-SY5Y cells, respectively. When we compared the standard protein sets between differentiated and undifferentiated SH-SY5Y neural cells, we found a total of 189 (Table 1) proteins common in both protein data sets with 86 statistically significantly differentiated proteins with $p < 0.05$. Among 86 significantly regulated proteins, 63 proteins displayed a significant upregulation, while 23 proteins were down-regulated. The Log_2 fold-change distribution of differentially regulated protein revealed seven proteins exhibiting a difference of 1-fold change [RS12 (40S ribosomal protein S12), RL10 (60S ribosomal protein L10), RL12 (60S ribosomal protein L12), DX39B (Spliceosome RNA helicase DDX39B), RSSA (40S ribosomal protein SA), CALX (Calnexin) and CALR (Calreticulin)], 21 proteins with the 0.5-fold change, 60 proteins showing 0.5-1 fold-change and 101 proteins with no statistical difference fold change (Fig. 1 (A)). On the other hand, the 6-OHDA treated differ-SH-SY5Y neural cells yielded 3636 proteins with 293 proteins shared the common data sets. When the protein profiles from the 6-OHDA treatment were compared with that of the untreated differentiated SH-SY5Y cells, a total of 188 proteins matched both protein data sets with a total of 101 proteins (Table 2) exhibited statistical significance difference. Among 101 significantly regulated proteins, 63 proteins upregulated, and 38 proteins downregulated. The Log2 fold-change distribution of differentially regulated proteins displays three proteins with the difference of 1-fold change [VDAC1 (Voltage-dependent anion-selective channel protein 1), HSPA9 (Stress-70 protein mitochondrial), HSPE1 (10 kDa heat shock protein mitochondrial)], 15 proteins with a 0.5-1 fold-change difference, 84 proteins showing 0.5-1 fold-change and 86 proteins with no statistical difference fold-change (Fig. 1(B)).

Biocomputational Analysis of differentially regulated proteins

Functional Annotation Analysis of differentially regulated proteins using PANTHER

To further elucidate the changes in cellular processes, the gene ontology (GO) analysis of the 86 differentially expressed proteins *($p < 0.05$)* in the differ-SH-SY5Y neural cells were investigated using the PANTHER bioinformatics database. These proteins were analysed based on changes in the GO term classification clusters' biological process, molecular function, and cellular component. The GO-molecular function of differ-SH-SY5Y neural cells showed a strong correlation to the structural modulation, activity and binding of ribosomes and ribosomal proteins. As for the GO-biological process, the differentially expressed proteins modulated the ribosomal assembly, biogenesis, glycolytic process (ATP generation) and DNA synthesis (purine nucleoside and ribonucleotide diphosphate phosphorylation and metabolic process). These molecular and biological processes were identified as concentrated at cytosolic ribosome units, as shown in the GO-cellular component (Fig. 2 (A)).

Next, for the 6-OHDA induced neurodegeneration in differ-SH-SY5Y, the GO-molecular function showed the association of the dysregulated proteins to the DNA structural alterations (structural molecule, purine, nucleoside, nucleotide), changes in structural constituents of ribosomes, metabolic processes (carbohydrate derivative binding), calcium cell signalling pathway (Calcium ion binding), metal ion homeostasis (metal ion binding) and unfolded protein binding. For the GO-biological process, the analysis revealed 6-OHDA induced neurodegeneration causes enrichment of the cellular mechanisms that identify and respond to misfolded/unfolded proteins (i.e., protein folding, cellular response to topologically incorrect protein, cellular response to unfolded proteins, endoplasmic reticulum unfolded protein response), metabolic activity (glycolytic activity, ATP generation), DNA structural changes (purine ribonucleoside diphosphate metabolic process) and apoptotic nucleosome assembly. The proteins localized in GO-cellular components were identified to be mitochondria (i.e., proton-transporting ATP synthase complex, mitochondrial prohibitin complex, mitochondria cristae), neuronal synapse or ribbon synapse (dense body), ribosome (i.e., eukaryotic translation elongation factor 1 complex, cytosolic RNA splicing (pIC1n-Sn protein complex, U7 snRNP) and endoplasmic reticulum (Fig. 2 (B)).

STRING Protein-protein interaction (PPI) networks analysis of differentially regulated proteins using STRING.

The STRING PPI network in differ-SH-SY5Y neural cells generated a total of 396 edges and 86 nodes with a PPI enrichment p-value of $< 1.00 \times 10^{-16}$), which was generated using the highest confidence (0.9) category (Fig. 3(A)). The PPI enrichment clusters showed a local clustering coefficient of 0.658. A total of three clusters were generated using K-means clustering. Proteins in **cluster I** include peroxiredoxin-6 (PRDX6), peroxiredoxin-5 mitochondrial (PRDX5), rho GDP-dissociation inhibitor 1 (ARHGDIA), peroxiredoxin-1 (PRDX1), 14-3-3 protein epsilon (YWHAE), 14-3-3 protein beta/alpha (YWHAB), 14-3-3 protein gamma (YWHAG), Rab GDP dissociation inhibitor beta (GDI2) and Glutathione S-transferase P (GSTP1) whilst proteins in **cluster II** comprises EEF1B2 (Elongation factor 1-beta), EEF2 (Elongation factor 2), EIF4A1 (Eukaryotic initiation factor 4A-I), PPP2RIA (Serine/threonine-protein phosphatase 2A 65 kDa regulatory subunit A alpha isoform), RPL10 (60S ribosomal protein L10), RPL10A (60S ribosomal protein L10a), RPL11 (60S ribosomal protein L11), RPL12 (60S ribosomal protein L12), RPL24 (Ribosomal protein L24), RPL27A (Ribosomal protein L27a), RPL4 (L ribosomal proteins), RPL6 (60S ribosomal protein L6), RPL7 (60S ribosomal protein L7), RPLP0 (60S acidic ribosomal protein P0), RPLP1 (60S acidic ribosomal protein P1), RPLP2 (60S acidic ribosomal protein P2), RPS12 (Ribosomal protein S12), RPS13 (Ribosomal protein S13), RPS25 (Ribosomal protein S25), RPS3 (40S ribosomal protein S3), RPS4X (Ribosomal protein S4), RPS5 (Ribosomal protein S5), RPS7 (40S ribosomal protein S7), RPS9 (Ribosomal protein S9), RPSA (40S ribosomal protein SA) and SRP14 (Signal recognition particle 14 kDa protein). **Cluster III** contains proteins such as DDX39B (Spliceosome RNA helicase DDX39B), FUS (RNA-binding protein FUS), HNRNPC (Heterogeneous nuclear ribonucleoproteins C1/C2), HNRNPD (Heterogeneous nuclear ribonucleoprotein D0), HNRNPK (Heterogeneous nuclear ribonucleoprotein K), HNRNPM (Heterogeneous nuclear ribonucleoprotein M), HSPA8 (Heat shock cognate 71 kDa protein), ILF2 (Interleukin enhancer-binding factor 2), RBMX (RNA-binding motif protein) and PCBP2 (Poly(rC)-

binding protein 2) (Fig. 3(A)). As cluster II exhibits the highest confidence edges with strong populated PPI, proteins in this cluster were further analysed for the pathway enrichment using the DAVID and KEGG databases.

The STRING PPI networks of the 6-OHDA induced neurodegeneration in differ-SH-SY5Y neural cells that generated a total of 245 edges and 97 nodes with PPI enrichment p-value $< 1.0 \times 10^{-16}$ is shown in Fig. 3(B). The networks were derived using the highest confidence (0.9) category that demonstrates three distinct clusters generated using K-means clustering. The PPI enrichment clusters exhibited a local clustering coefficient of 0.676 that generated three distinct clusters using K-means clustering. Proteins in cluster I include CALR (calreticulin), CANX (calnexin), HSP90B1 (endoplasmin), HSPA5 (78 kDa glucose-regulated protein), HSPA9 (stress-70 protein, mitochondrial), HSPD1 (60 kDa heat shock protein), HSPE1 (10 kDa heat shock protein), PDIA3 (protein disulfide-isomerase A3), PDIA6 (protein disulfide-isomerase A6), PPIB (peptidyl-prolyl cis-trans isomerase B), SLC25A5 (ADP/ATP translocase 2), VDAC1 (voltage-dependent anion-selective channel protein 1), VDAC2 (voltage-dependent anion-selective channel protein 2), VDAC3 (voltage-dependent anion-selective channel protein 3), ATP5A1 (ATP synthase subunit alpha, mitochondrial), ATP5B (ATP synthase subunit beta, mitochondrial) ATP5D (ATP synthase subunit delta, mitochondrial) and VGF (neurosecretory protein VGF). Cluster II includes RPL4 (L ribosomal proteins), RPS16 (Ribosomal protein S16), RPS6 (40S ribosomal protein S6), RPS15 (Ribosomal protein S15), RPS25 (40S ribosomal protein S25), RPS16 (40S ribosomal protein S16), RPL23 (60S ribosomal protein L23), EEF1A1 (Elongation factor 1-alpha 1), EEF2 (Elongation factor 2), RPS7 (40S ribosomal protein S7), EEF1A2 (Elongation factor 1-alpha 2), whilst proteins in cluster III include histone proteins such as H2AFX (Histone H2AX), H2AFY (Core histone macro-H2A.1), H2AFY2 (Core histone macro-H2A.2), H2BFS (Histone H2B type F-S), HIST1H2BB (Histone H2B type 1-B), HIST1H2BC (Histone H2B type 1-C), HIST1H2BD (Histone H2B type 1-D), HIST1H2BH (Histone H2B type 1-H), HIST1H2BJ (Histone H2B type 1-J), HIST1H2BK (Histone H2B type 1-K), HIST1H2BM (Histone H2B type 1-M), HIST1H2BN (Histone H2B type 1-N), HIST1H2BO (Histone H2B type 1-O), HIST1H3A (Histone cluster 1 H3 family member a), HIST1H4A (Histone cluster 1 H4 family member a), HIST2H2BE (Histone H2B type 2-E), HIST2H2BF (Histone H2B type 2-F), RAN (GTP-binding nuclear protein Ran) and TRIM28 (Transcription intermediary factor 1-beta). The strong PPI edges and highest number of protein recruitment were noted in cluster III compared to other clusters; hence proteins populated in this cluster were subjected for pathway enrichment analysis.

Discussion

In this study, the differentially expressed proteins in differ-SH-SY5Y neural cells and the cellular model of PD were identified, and the alteration of the proteome was assessed through the enrichment of molecular functions, biological processes, and cellular pathways. Our findings showed that the RA induced differentiation of SH-SY5Y cells exhibited a significant increase in the expression of two crucial proteins, calnexin and calreticulin proteins (Fig. 1(A)). Calreticulin, an essential Ca^{2+} binding chaperone in the endoplasmic reticulum, is a vital entity of the calreticulin/calnexin cycle (Xiao et al. 2017). Nevertheless,

the calreticulin/calnexin cycle plays a crucial role in folding newly synthesized proteins for cellular differentiation or organ development (Dudek and Michalak 2013). Emerging studies have shown that calreticulin mediated suppression of oncogenic N-MYC (MYCN) resulted in increased neurite length and differentiation marker GAP-43 (Lee et al. 2019). A study on the calreticulin knock-out mouse model displayed embryonic lethality with remarkable defects in the heart, brain and body wall, suggesting the pivotal role of calreticulin in developing the nervous system (Rauch et al. 2000). On the other hand, calnexin's role has been associated with nerve cells' myelination as being deficient in the calnexin gene leads to myelinopathy (Kraus et al. 2010). Hence, the expression of these proteins in differ-SH-SY5Y neural cells signifies the activation of neuronal features such as myelination and suppression of oncogenic characteristics of neuroblastoma cells.

The differ-SH-SY5Y neural cells also demonstrated a significant 1-fold down-regulation of DDX39B and ribosomal proteins, RPS12, RPL10, RPL12 and RPSA. The DDX39B is a member of the DEAD-box family of RNA helicases that plays a pivotal role in pre-mRNA splicing and mRNA export to the cytoplasm (Zhang et al. 2018). Intrinsically, the DDX39B promotes the unwinding of the U4/U6 snRNA duplex, which in-turn permits the binding of the U2 snRNP to the pre-mRNA in a series of ATP-dependent pre-mRNA splicing process (Shen et al. 2008). Consequently, DDX39B mediates the nuclear transport of mRNA by facilitating the interaction between THO complex and CIP29 and Aly (nuclear factors) (Folco et al. 2012). The interaction between the DDX39B with export proteins CIP29 and Aly during the formation of the conserved TREX mRNA export complex is controlled by ATP hydrolysis (K et al. 2010). A recent study has reported that the increased pre-ribosomal RNA levels of DDX39B augment global translation and cell proliferation of diverse cancer types. This study also showed that DDX39B knockdown cells displayed a significantly reduced stability of pre-ribosomal 47S RNA, whereas the 47S rRNA stability was unaltered in DDX39B overexpressed cells (Awasthi et al. 2018). The present study's findings suggest that the down-regulation of DDX39B in differ-SH-SY5Y neural cells is closely linked to the suppression of ribosomal proteins and RNA biogenesis. The inhibition of cell proliferation in differentiated neural cells was caused by the suppression of ribosomal proteins that play a crucial role in protein biosynthesis and cell growth. Evidence supporting this finding comes from a study by Linstrom *et al*. that suggested that silencing of ribosomal protein S9 (RPS9) elicits cell proliferation restriction mediated by the p53 tumour suppressor pathway in cancer cells. This study also pointed out that the suppression of ribosomal proteins effectively promotes differentiation processes, senescence, or apoptosis in rapidly propagating cancer cells (Lindström and Nistér 2010). According to our STRING PPI analysis, a total of 28 differentially regulated proteins were found to form the most prominent network in cluster II. Among these, 21 ribosomal proteins displayed a significant down-regulation in differ-SH-SY5Y neural cells compared to undifferentiated SH-SY5Y cells (Fig. 4 (A&B)). These 21 ribosomal proteins were identified to have a pivotal role in the ribosome bio-pathway as curated by the KEGG database.

The ribosome is the cellular translational machinery's principal component that decodes messenger RNA (mRNA) to produce an amino acid chain through a complementary anticodon sequence (Guimarães 2017). The manufacture of this machinery component is known as ribosome biogenesis and occurs in the nucleolus via initiation by the RNA-polymerase-1 (RNA-pol1) that mediates the transcription of rRNA

genes (Drygin et al. 2010). Three RNA polymerase enzymes, RNA-pol1, RNA-pol2, RNA-pol3 and non-ribosomal factors, were responsible for generating the 90S pre-ribosomes in the nucleolus undergoes several modifications before splitting into pre-60S and pre-40S particles (Torreira et al. 2017). These particles mature into the large (60S) and small (40S) subunits for protein synthesis during the transportation from nucleolus into cytoplasm compartments through dissociation from most of the non-ribosomal factors (Delavoie et al. 2019). Emerging studies have revealed that ribosome biogenesis and protein translations are exceptionally synchronized with cellular processes, including cell division, differentiation and growth (Zhou et al., 2015). Disruption in any of these two dynamic processes could impede the crucial cellular biological processes and well-being.

Furthermore, recent pieces of evidence have documented that down-regulation of the ribosomal proteins (RPs) and translation efficiency during the differentiation process contribute to reduced cell growth (Marcon et al. 2017) (Bevort and Leffers 2000) (Hayashi et al. 2014). Bevort and Leffers have reported that 31 out of 32 RPs analysed were significantly suppressed in neuronal differentiation in human NTERA2 cells induced by retinoic acid. The same study also demonstrated that the reduction in RP mRNA expression was well correlated with inhibition of the proliferation marker known as proliferating cell nuclear antigen (PCNA) (Bevort and Leffers 2000). An incredible wealth of information was contributed by Hayashi *et al.*, elucidating the association between down-regulation of rRNA transcription and cellular differentiation (Hayashi et al. 2014). According to this report, the rRNA transcription was deliberately down-regulated using actinomycin D, a siRNA for Pol 1-specific transcription factor IA (TIF-IA) in HL-60 and THP-1 cells differentiation potential. The attenuation of rRNA transcription was shown to enhance the cell differentiation in both cell lines and increase the differentiation marker, CD11b. They also evaluated if cell differentiation was triggered by inhibition of the cell cycle since rRNA transcription is tightly paired with cell growth. The outcome of this study showed that cell cycle arrest that occurred without affecting rRNA transcription did not stimulate differentiation in mouse hematopoietic stem cells (Hayashi et al. 2014). This data is in line with our findings that showed a significant down-regulation of RPs in differ-SH-SY5Y cells indicate the augmentation in the differentiation mechanism and suppression of cell growth compared to undifferentiated SH-SY5Y neuroblastoma cells.

The neurotoxin 6-OHDA induced neurodegeneration model is a well-acknowledged neurodegenerative “simulation” conceived by the PD research community to study the disease cellular and molecular processes, both *in vitro* or *in vivo* settings (Xicoy et al. 2017). Although the model does not demonstrate the classical pathological hallmark of PD, which is the accumulation of α-synuclein and Lewy bodies, it expresses the cardinal processes in PD, including mitochondrial dysfunction, apoptosis, ROS induced oxidative stress, neuro-inflammation, lipid peroxidation and disruption in endogenous antioxidant enzymes (Dias et al. 2013). In our study, the 6-OHDA exposure on the differ-SH-SY5Y neural cells revealed a remarkable 1-fold change overexpression of VDAC1, HSPE1 and HSPA9 proteins (Fig. 1 (B)).

The VDAC1 is found abundantly on the outer membrane of mitochondria and functions as a gatekeeper for the passage of ions ($Ca^{2+,}$ K^{+}, Na^{+}) and metabolite substrates ATP, ADP and Pi (Camara et al. 2017). The conformational states of VDAC1 are voltage-dependent and ion selectivity, exhibiting a preference to

metabolite anions in high voltage conductance (open state) and cations in low voltage conductance (closed state) (Rostovtseva and Colombini 1997). The VDAC remains in high conductance or open state during mitochondria depolarization potential in the voltage range of about − 40 to + 40 mV (Hodge and Colombini 1997). The VDAC function is associated with NADH's oxidation, hence playing a pivotal role in mitochondria-mediated apoptotic signalling via interaction with pro-and anti-apoptotic mediators (Shoshan-Barmatz et al. 2017). Previous studies have reported that the overexpression of VDAC1 in cells undergoing apoptosis was mediated by increased cytosolic CA^{2+} level. Pro-apoptosis inducer such as hydrogen peroxide on Hela (human cervical adenocarcinoma) cells resulted in increased cytosolic Ca^{2+} and overexpressed oligomerised VDAC1 mediates the release of cytochrome c and apoptosis (Shoshan-Barmatz et al. 2017). Another study has further proven than a binding partner known as tubulin polymerization-promoting protein family member-3 (TPP3) promoted the oligomerisation of VDAC1 in palmitic acid-induced apoptosis of endothelial cells (Liu et al. 2020). Hence, the upregulation of VDAC1 protein expression in our finding indicates that the 6-OHDA treated differ-SH-SY5Y neural cells underwent rigorous oxidative stress-induced apoptosis, which is an expected outcome in a PD disease model.

The heat shock proteins (HSPs) are the most conserved 10kDa evolutionary proteins known as stress-inducible proteins. The HSPE1 (HSP10) is found abundantly in mitochondria, whereas HSPA9 (HSP70) exists in the cytoplasm and nucleus. Generally, HSPs functions as cytoprotective proteins with related co-chaperones under increased free radicals induced apoptosis through the initiation of a repair mechanism and refolding of misfolded peptides, possible proteolysis of irreparable proteins, signalling transduction and translocation (Sharma et al. 2012). Principally, the HSPA9 assists in the transportation of nuclear-encoded proteins to the mitochondria and these proteins are subsequently refolded by HSPD1(HSP60) and its co-chaperone, HSPE1 (Voos 2013). The HSPD1-HSPE1 complex chaperonin consists of two rings arranged to conform to a barrel-shaped structure with a central cavity. This complex receives the unfolded or misfolded proteins into its central cavity and facilitates the folding process divided into three steps. In the first step, the HSPD1-HSPE1 complex binds firmly with the unfolded or misfolded proteins; then the proteins get trapped in the central cavity capped by HSPE1 refolding of the protein takes place. Finally, the correctly folded proteins are ejected from the chaperonin complex. The unfolded or partially folded proteins are redirected to the chaperonin to repeat the entire cycle until the correctly folded proteins are achieved (Jia et al. 2011). While the HSPD1 and HSPE1 are crucial housekeeping proteins for efficient mitochondria function and biogenesis, the HSPA9 is best known for its cytosolic chaperone activity in assisting protein folding, degradation and translocation. Overwhelming evidence has pointed out that HSPs have been identified to be involved in multiple pathways in promoting the anti-apoptosis effect (Ikwegbue et al. 2018). According to Li *et al.*, the chaperone activity of HSPA9 is crucial for the inhibition of caspase activation at a reaction point between the cytochrome c release and caspase-3 activation (Li et al. 2000). The overexpression of HSPA9 was also reported to indirectly inhibit the stress-induced apoptosis by preventing the conformational change and translocation of Bax into mitochondria, indicating the suppression of apoptosis through Bax inactivation and inhibition of caspase activation (Stankiewicz et al. 2005). A recent study has clarified that overexpression of HSPA9 prevents inflammation in a rat model of intracerebral haemorrhage through inhibition of inflammatory cytokines

such as TNF-α, IL-β, Bax and increased Bcl-2 levels (Lv et al. 2017). Hence, we postulate that the overexpression of HSPE1 and HSPA9 in our study is closely connected to the cytoprotective mechanism of the neuronal cells to inhibit the avalanche of apoptotic mediators released in response to 6-OHDA treatment. HSP expression in the PD cell model is an important biomarker that paves the way for future studies in developing potential therapies targeting the HSPE1 and HSPA9 to mitigate apoptosis-induced cell death.

The treatment of 6-OHDA induced neurodegeneration on differ-SH-SY5Y neural cells resulted in an enrichment of 4 clusters or pathways in STRING PPI analysis (Fig. 3(B)). The crosstalk between proteins populated in cluster IV of STRING PPI displaying the most prominent interaction was further investigated using KEGG pathway enrichment analysis. The KEGG bioinformatic pathway enrichment database predicted the systemic lupus erythematosus (SLE) pathway with the involvement of 17 out of 19 upregulated proteins (Fig. 5(A) and (B)). SLE is an autoimmune disease of unknown aetiology that primarily affects women in the childbearing age (Pieterse and van der Vlag 2014). The disease is characterized by disturbances of the immune system that arise when the immune cells respond to self-antigens, mainly nuclear constituents, i.e., histones, ribonucleoproteins and DNA (Pradhan et al. 2010). For over two decades, apoptosis has been regarded as a significant source of autoantigens in SLE. Apoptosis can be actively triggered by ligation of cell surface receptors, including Fas and tumour necrosis factor receptor (TNFR) or passively via deficient in crucial cell survival signals (De Wilde et al. 2001). Apoptotic cells undergo an orderly process of morphological alterations, such as nuclear chromatin condensation, nuclear splitting, cytoskeletal disruption, cell shrinkage and membrane blebbing (Saraste and Pulkki 2000). Persistent exposure of the immune system to apoptotic bodies leads to the formation of an anti-chromatin/chromatin complex, triggering an array of inflammation in multiple organs in SLE patients. Previous studies have shown that autoantibodies' increased reactivity against histone proteins, namely histone H4 and H2B peptides, correlated with SLE disease activity (Dieker et al. 2016). Whereas in PD, the selective vulnerability of dopamine neurons to environmental toxins, intracellular accumulations of highly oxidative free radical and toxic accumulation of misfolded proteins leads to neurodegeneration (apoptosis) and activation of neuro-inflammation pathway (Hald and Lotharius 2005). As such, the neuro-inflammation pathway is triggered through activation of microglia or the "immune cell of the brain", which releases the pro-inflammatory mediators including tumour necrosis factor (TNF-α), interleukin (IL-1β), IL-2, IL-4, interferon (IFN-γ) and nitric oxide (NO) (Liu et al. 2019). The pro-inflammatory mediators instigate further detrimental effects on nigral neurons by causing direct toxicity in neurons and induce ongoing neuro-inflammation through microglial NO activation (Jung et al. 2019). Emerging studies have reported that chronic SLE patients presented with parkinsonian syndromes, including slowness in movement, adiadochokinesia, postural rigidity and tremor (Fabiani et al. 2002).

In our study, the histone proteins were shown to be exceptionally overexpressed in 6-OHDA induced neurodegeneration on differ-SH-SY5Y neural cells (PD cell model). Structurally, histone proteins exist as an octamer with two copies of each of the four core histone proteins H2A, H2B, H3 and H4 and two linker histones, H1 and H5 (Andrews and Luger 2011). The 147bp of DNA packages the octamer histones to form a nucleosome. The four core histones form a conserved central motif domain known as histone fold

composed of a long central α-helix structure with a short helix flanked on either side (Jiang and Pugh 2009). In comparison, the linker histone associates with nucleosome to transform nucleosomes into various high-order chromatin structures. Ideally, the histone proteins function in constructing the nucleus and fine-tuning gene expression for physiological and pathological processes (Martire and Banaszynski 2020). An increasing body of evidence suggests that besides regulating nucleosome dynamics, histone proteins are released in the extracellular field by cells undergoing apoptosis (Silk et al. 2017).

It is well established that chromatin condensation coupled with DNA fragmentation is important nuclear events during apoptosis (He et al. 2009). In response to apoptotic signals, the core and linker histones are detached from genomic DNA and released into cytoplasmic and extracellular regions. Wu *et al.* have reported that the timing of histone release from genomic DNA directly correlated with the advancement of the apoptosis process (Wu et al. 2002). The release of histone proteins and DNA-bound nucleosomes into the intracellular space by damaged DNA is an essential indicator of apoptosis-activated pro-inflammatory cascades (Silk et al. 2017). Once in the cytosol, histones act as a member of the damage-associated molecular pattern molecules (DAMPs), activating immune response and causing additional cytoproliferative effects (Xu et al. 2009). Along these lines, studies have revealed that core histones such as H2A, H2B, H3, H4 and linker histone H1 are frequently detected in neurons (Mishra et al. 2010), microglia (Klein et al. 2014) and macrophages (Brix et al. 1998) in response to oxidative stress (Hu et al. 2018). Notably, the degree of circulating histone and nucleosomes are elevated in cancer, infection and inflammation proposing histone as an essential biomarker in human diseases (Chen *et al.*, 2014). Hence, the upregulation of a set of histone proteins in 6-OHDA induced neuronal death in our study is a clear indication of chromatin condensation and modification during DNA fragmentation in the apoptosis process.

In conclusion, the PD cell model is an essential *in vitro* platform for investigating the molecular and biological processes involved in the disease process and paving the way for future discoveries of potential therapeutic drugs that reverse these mechanisms. Ideally, a disease model should express the biomarkers that indicate the progression of PD's pathological conditions such as mitochondrial dysfunction, DNA fragmentation, neurodegeneration, and neuro-inflammation. The differ-SH-SY5Y neural cells developed from SH-SY5Y human neuroblastoma cells expressed substantial dopaminergic markers and, upon perturbation with 6-OHDA, displayed pathological changes frequently detected in PD. The differentially regulated proteins were analysed using GO functional annotation, STRING PPI and KEGG pathway enrichment databases to understand the cellular machinery's alterations during the disease process. We suggest that the down-regulation of the ribosome pathway promotes the differentiation of neuronal cells. In contrast, the neurodegeneration process is mediated by nucleosomal degradation demonstrated by the upregulation of histone products in the SLE pathway as a significant PD event.

Declarations

Ethics approval and consent to participate: Not Applicable

Consent for publication: Permission obtained from Kanehisa Laboratories to publish the KEGG pathway map images both in prints and digital under the CC BY 4.0 open access license.

Availability of data and materials: Not Applicable

Competing interests: There are no ethical/legal conflicts involved in the article.

Funding: This study was supported by the International Medical University, Kuala Lumpur research grant (Grant: IMU R 194 2016).

Authors' contributions: **KBM** performed all experiments and prepared the manuscript, **AR** and **HN** designed the overall study. **AR** and **SDS** involved in project administration. **PR** assisted in data analysis. All authors read and approved the final manuscript.

Acknowledgements: The authors thank Dr Shafiq Asnawi (Proteomic laboratory Jeffrey Cheah School of Medicine, Monash University Malaysia) for technical support in carrying out the LC-MS/MS analysis.

Authors' information: [1]School of Postgraduate Studies, International Medical University, Kuala Lumpur, Malaysia, [2]Jeffrey Cheah School of Medicine and Health Sciences, Monash University, Malaysia, Bandar Sunway, Malaysia, [3]Pathology Division, School of Medicine, International Medical University, Kuala Lumpur, Malaysia, [4]Division of Applied Biomedical Sciences and Biotechnology, School of Health Sciences, International Medical University, Kuala Lumpur, Malaysia, [5]College of Public Health, Medicine and Veterinary Sciences, James Cook University, Townsville, Queensland 4811, Australia, [6]Monash-Industry Palm Oil Education and Research Platform (MIPO), Monash University Malaysia, Bandar Sunway, Selangor, Malaysia

References

1. Andrews AJ, Luger K (2011) Nucleosome structure(s) and stability: Variations on a theme. Annu Rev Biophys 40:99–117. https://doi.org/10.1146/annurev-biophys-042910-155329
2. Awasthi S, Chakrapani B, Mahesh A et al (2018) DDX39B promotes translation through regulation of pre-ribosomal RNA levels. RNA Biol 15:1157–1166. https://doi.org/10.1080/15476286.2018.1517011
3. Beere HM, Wolf BB, Cain K et al (2000) Heat-shock protein 70 inhibits apoptosis by preventing recruitment of procaspase-9 to the Apaf-1 apoptosome. Nat Cell Biol 2:469–475. https://doi.org/10.1038/35019501
4. Bevort M, Leffers H (2000) Down regulation of ribosomal protein mRNAs during neuronal differentiation of human NTERA2 cells. Differentiation 66:81–92. https://doi.org/10.1046/j.1432-0436.2000.660203.x
5. Brix K, Summa W, Lottspeich F, Herzog V (1998) Extracellularly occurring histone H1 mediates the binding of thyroglobulin to the cell surface of mouse macrophages. J Clin Invest 102:283–293.

https://doi.org/10.1172/JCI1614

6. Camara AKS, Zhou YF, Wen PC et al (2017) Mitochondrial VDAC1: A key gatekeeper as potential therapeutic target. Front Physiol 8:460
7. De Wilde G, Murray-Rust J, Boone E et al (2001) Structure-activity relationship of the p55 TNF receptor death domain and its lymphoproliferation mutants. Eur J Biochem 268:1382–1391. https://doi.org/10.1046/j.1432-1327.2001.02004.x
8. Delavoie F, Soldan V, Rinaldi D et al (2019) The path of pre-ribosomes through the nuclear pore complex revealed by electron tomography. Nat Commun 10:1–12. https://doi.org/10.1038/s41467-019-08342-7
9. Dias V, Junn E, Mouradian MM (2013) The role of oxidative stress in parkinson's disease. J Parkinsons Dis 3:461–491
10. Dieker J, Berden JH, Bakker M et al (2016) Autoantibodies against Modified Histone Peptides in SLE Patients Are Associated with Disease Activity and Lupus Nephritis. PLoS One 11:e0165373. https://doi.org/10.1371/journal.pone.0165373
11. Drygin D, Rice WG, Grummt I (2010) The RNA polymerase i transcription machinery: An emerging target for the treatment of cancer. Annu Rev Pharmacol Toxicol 50:131–156
12. Dudek E, Michalak M (2013) Calnexin and Calreticulin. In: Encyclopedia of Metalloproteins. Springer New York, pp 555–562
13. El-Rami F, Nelson K, Xu P (2017) Proteomic Approach for Extracting Cytoplasmic Proteins from Streptococcus sanguinis using Mass Spectrometry. J Mol Biol Res 7:50. https://doi.org/10.5539/jmbr.v7n1p50
14. Fabiani G, Teive HAG, Germiniani FMB et al (2002) Reversible Parkinsonian syndrome in systemic and brain vasculitis. Mov Disord 17:601–604. https://doi.org/10.1002/mds.10029
15. Folco EG, Lee C-S, Dufu K et al (2012) The Proteins PDIP3 and ZC11A Associate with the Human TREX Complex in an ATP-Dependent Manner and Function in mRNA Export. PLoS One 7:e43804. https://doi.org/10.1371/journal.pone.0043804
16. Guimarães RC (2017) Self-referential encoding on modules of anticodon pairs–Roots of the biological flow system. Life 7
17. Hald A, Lotharius J (2005) Oxidative stress and inflammation in Parkinson's disease: Is there a causal link? Exp. Neurol 193:279–290
18. Hayashi Y, Kuroda T, Kishimoto H et al (2014) Downregulation of rRNA Transcription Triggers Cell Differentiation. PLoS One 9:e98586. https://doi.org/10.1371/journal.pone.0098586
19. He B, Lu N, Zhou Z (2009) Cellular and nuclear degradation during apoptosis. Curr Opin Cell Biol 21:900–912
20. Hodge T, Colombini M (1997) Regulation of metabolite flux through voltage-gating of VDAC channels. J Membr Biol 157:271–279. https://doi.org/10.1007/s002329900235

21. Hu J, Han J, Li H et al (2018) Human Embryonic Kidney 293 Cells: A Vehicle for Biopharmaceutical Manufacturing, Structural Biology, and Electrophysiology. Cells Tissues Organs 205:1–8
22. Ikwegbue PC, Masamba P, Oyinloye BE, Kappo AP (2018) Roles of heat shock proteins in apoptosis, oxidative stress, human inflammatory diseases, and cancer. Pharmaceuticals 11
23. Jia H, Halilou AI, Hu L et al (2011) Heat shock protein 10 (Hsp10) in immune-related diseases: One coin, two sides. Int J Biochem Mol Biol 2:47–57
24. Jiang C, Pugh BF (2009) Nucleosome positioning and gene regulation: Advances through genomics. Nat Rev Genet 10:161–172
25. Jung YJ, Tweedie D, Scerba MT, Greig NH (2019) Neuroinflammation as a Factor of Neurodegenerative Disease: Thalidomide Analogs as Treatments. Front. Cell Dev. Biol. 7
26. K D, MJ L, J S, et al (2010) ATP is required for interactions between UAP56 and two conserved mRNA export proteins, Aly and CIP29, to assemble the TREX complex. Genes Dev 24:. https://doi.org/10.1101/GAD.1898610
27. Klein B, Lütz-Meindl U, Kerschbaum HH (2014) From the nucleus to the plasma membrane: Translocation of the nuclear proteins histone H3 and lamin B1 in apoptotic microglia. Apoptosis 19:759–775. https://doi.org/10.1007/s10495-014-0970-7
28. Kraus A, Groenendyk J, Bedard K et al (2010) Calnexin deficiency leads to dysmyelination. J Biol Chem 285:18928–18938. https://doi.org/10.1074/jbc.M110.107201
29. Lee ACL, Shih YY, Zhou F et al (2019) Calreticulin regulates MYCN expression to control neuronal differentiation and stemness of neuroblastoma. J Mol Med 97:325–339. https://doi.org/10.1007/s00109-018-1730-x
30. Li CY, Lee JS, Ko YG et al (2000) Heat shock protein 70 inhibits apoptosis downstream of cytochrome c release and upstream of caspase-3 activation. J Biol Chem 275:25665–25671. https://doi.org/10.1074/jbc.M906383199
31. Lindström MS, Nistér M (2010) Silencing of Ribosomal Protein S9 Elicits a Multitude of Cellular Responses Inhibiting the Growth of Cancer Cells Subsequent to p53 Activation. PLoS One 5:e9578. https://doi.org/10.1371/journal.pone.0009578
32. Liu CY, Wang X, Liu C, Zhang HL (2019) Pharmacological Targeting of Microglial Activation: New Therapeutic Approach. Front. Cell. Neurosci. 13
33. Liu N, Li Y, Nan W et al (2020) Interaction of TPPP3 with VDAC1 Promotes Endothelial Injury through Activation of Reactive Oxygen Species. Oxid Med Cell Longev 2020:. https://doi.org/10.1155/2020/5950195
34. Lv LJ, Li J, Qiao HB et al (2017) Overexpression of GRP75 inhibits inflammation in a rat model of intracerebral hemorrhage. Mol Med Rep 15:1368–1372. https://doi.org/10.3892/mmr.2017.6126
35. Magalingam KB, Radhakrishnan AK, Somanath SD et al (2020) Influence of serum concentration in retinoic acid and phorbol ester induced differentiation of SH-SY5Y human neuroblastoma cell line. Mol Biol Rep. https://doi.org/10.1007/s11033-020-05925-2

36. Marcon BH, Holetz FB, Eastman G et al (2017) Downregulation of the protein synthesis machinery is a major regulatory event during early adipogenic differentiation of human adipose-derived stromal cells. Stem Cell Res 25:191–201. https://doi.org/10.1016/j.scr.2017.10.027
37. Martire S, Banaszynski LA (2020) The roles of histone variants in fine-tuning chromatin organization and function. Nat Rev Mol Cell Biol 21:522–541
38. Mishra B, Von Der Ohe M, Schulze C et al (2010) Functional role of the interaction between polysialic acid and extracellular histone H1. J Neurosci 30:12400–12413. https://doi.org/10.1523/JNEUROSCI.6407-09.2010
39. Pieterse E, van der Vlag J (2014) Breaking immunological tolerance in systemic lupus erythematosus. Front Immunol 5:164
40. Pradhan VD, Patwardhan MM, Ghosh K (2010) Anti-nucleosome antibodies as a disease marker in systemic lupus erythematosus and its correlation with disease activity and other autoantibodies. Indian J Dermatol Venereol Leprol 76:145–149. https://doi.org/10.4103/0378-6323.60558
41. Rauch F, Prud'Homme J, Arabian A et al (2000) Heart, brain, and body wall defects in mice lacking calreticulin. Exp Cell Res 256:105–111. https://doi.org/10.1006/excr.2000.4818
42. Rostovtseva T, Colombini M (1997) Vdac channels mediate and gate the flow of ATP: Implications for the regulation of mitochondrial function. Biophys J 72:1954–1962. https://doi.org/10.1016/S0006-3495(97)78841-6
43. Saraste A, Pulkki K (2000) Morphologic and biochemical hallmarks of apoptosis. Cardiovasc Res 45:528–537
44. Sharma GT, Nath A, Prasad S et al (2012) Expression and Characterization of Constitutive Heat Shock Protein 70.1 (HSPA-1A) Gene in In Vitro Produced and In Vivo-Derived Buffalo (Bubalus bubalis) Embryos. Reprod Domest Anim 47:975–983. https://doi.org/10.1111/j.1439-0531.2012.02002.x
45. Shen H, Zheng X, Shen J et al (2008) Distinct activities of the DExD/H-box splicing factor hUAP56 facilitate stepwise assembly of the spliceosome. Genes Dev 22:1796–1803. https://doi.org/10.1101/gad.1657308
46. Shoshan-Barmatz V, Maldonado EN, Krelin Y (2017) VDAC1 at the crossroads of cell metabolism, apoptosis and cell stress. Cell Stress 1:11–36
47. Silk E, Zhao H, Weng H, Ma D (2017) The role of extracellular histone in organ injury. Cell Death Dis 8:e2812
48. Stankiewicz AR, Lachapelle G, Foo CPZ et al (2005) Hsp70 inhibits heat-induced apoptosis upstream of mitochondria by preventing Bax translocation. J Biol Chem 280:38729–38739. https://doi.org/10.1074/jbc.M509497200
49. Torreira E, Louro JA, Pazos I et al (2017) The dynamic assembly of distinct RNA polymerase i complexes modulates rDNA transcription. Elife 6:. https://doi.org/10.7554/eLife.20832
50. Voos W (2013) Chaperone-protease networks in mitochondrial protein homeostasis. Biochim Biophys Acta - Mol Cell Res 1833:388–399

51. Wu D, Ingram A, Lahti JH et al (2002) Apoptotic release of histones from nucleosomes. J Biol Chem 277:12001–12008. https://doi.org/10.1074/jbc.M109219200
52. Xiao X, Chen C, Yu T-M et al (2017) Molecular Chaperone Calnexin Regulates the Function of Drosophila Sodium Channel Paralytic. Front Mol Neurosci 10:57. https://doi.org/10.3389/fnmol.2017.00057
53. Xicoy H, Wieringa B, Martens GJM (2017) The SH-SY5Y cell line in Parkinson's disease research: a systematic review. Mol Neurodegener 12:1–11. https://doi.org/10.1186/s13024-017-0149-0
54. Xu J, Zhang X, Pelayo R et al (2009) Extracellular histones are major mediators of death in sepsis. Nat Med 15:1318–1321. https://doi.org/10.1038/nm.2053
55. Zhang L, Yang Y, Li B et al (2018) The DEAD-box RNA helicase Ddx39ab is essential for myocyte and lens development in zebrafish. https://doi.org/10.1242/dev.161018
56. Zhou X, Liao W-J, Liao J-M et al Ribosomal proteins: functions beyond the ribosome. https://doi.org/10.1093/jmcb/mjv014

Tables

Due to technical limitations, table 1 & 2 is only available as a download in the Supplemental Files section.

Figures

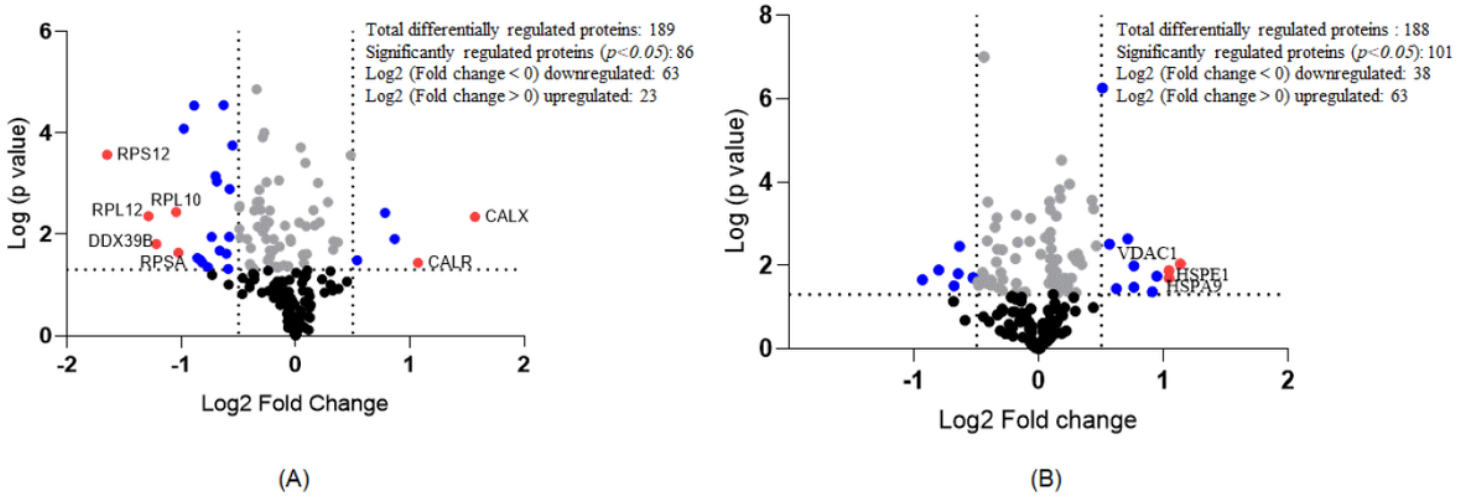

Figure 1

Quantitative proteomic analysis of neuronal development and 6-OHDA induced neurodegeneration on differ-SH-SY5Y neural cells. Volcano plot shows the differentially regulated protein in (A) Differ-SH-SY5Y neural cells (B) 6-OHDA induced neurodegeneration in differ-SH-SY5Y neural cells. The horizontal coordinate (x-axis) represents the difference in fold change (logarithmic transformation at the base of 2), and the vertical coordinate (Y-axis) is the significant difference of p-value (logarithmic transformation at

the base of 10). Proteins that are 1-fold significantly regulated are presented as red dots, while those that had 0.5 to 1-fold change are shown as blue dots. Proteins with fold change less than 0.5-fold change are presented as grey dots. Black dots represent proteins that do not have a statistically significant fold-change.

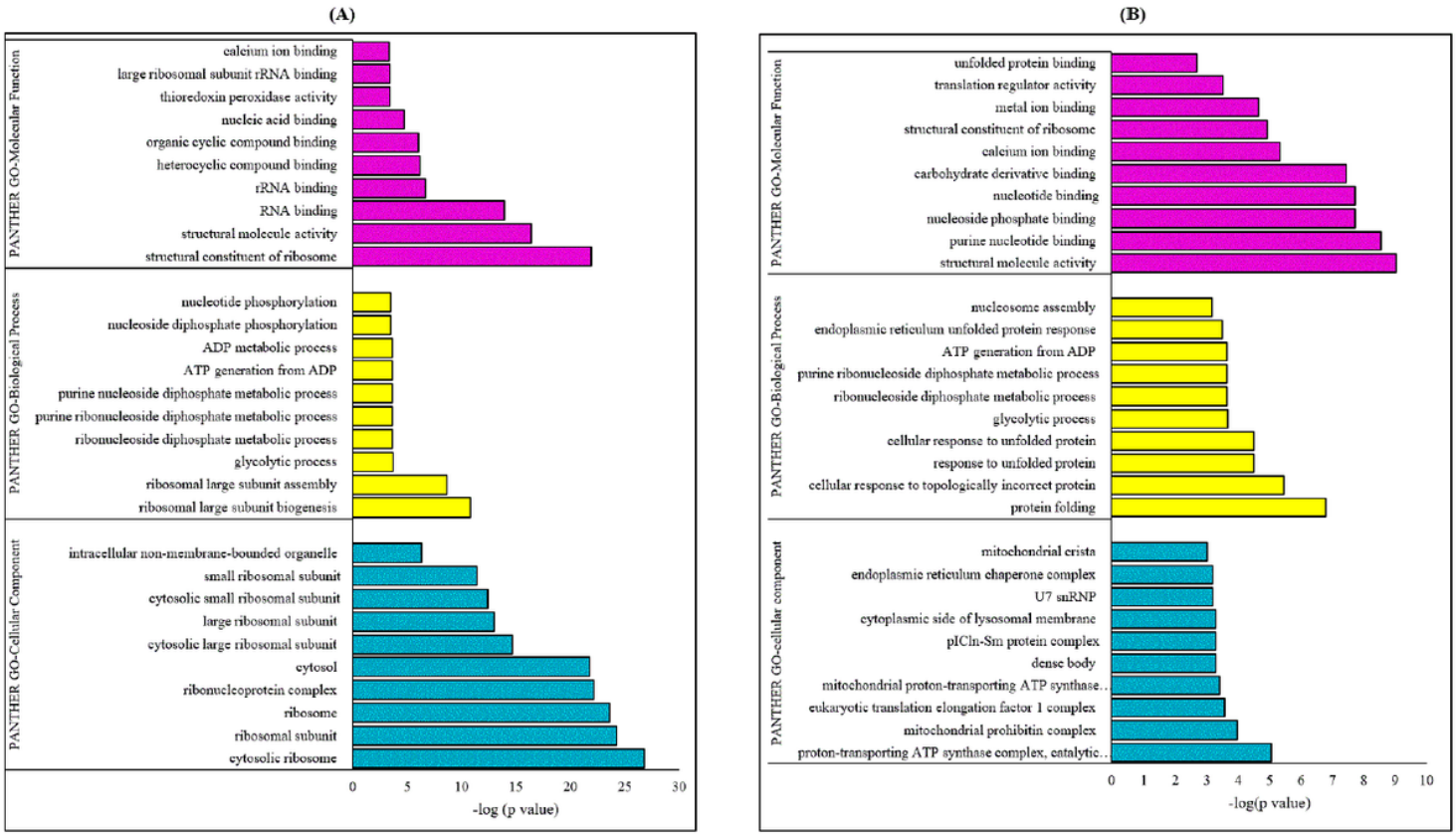

Figure 2

Gene ontology (GO) functional annotation analysis. The GO classification terms of molecular function, biological process and cellular component using PANTHER online database on Differentially regulated proteins ($p<0.05$) in (A) Differ-SH-SY5Y neural cells in comparison with undifferentiated SH-SY5Y cells and (B) 6-OHDA treated differ-SH-SY5Y cells in comparison with untreated differ-SH-SY5Y cells.

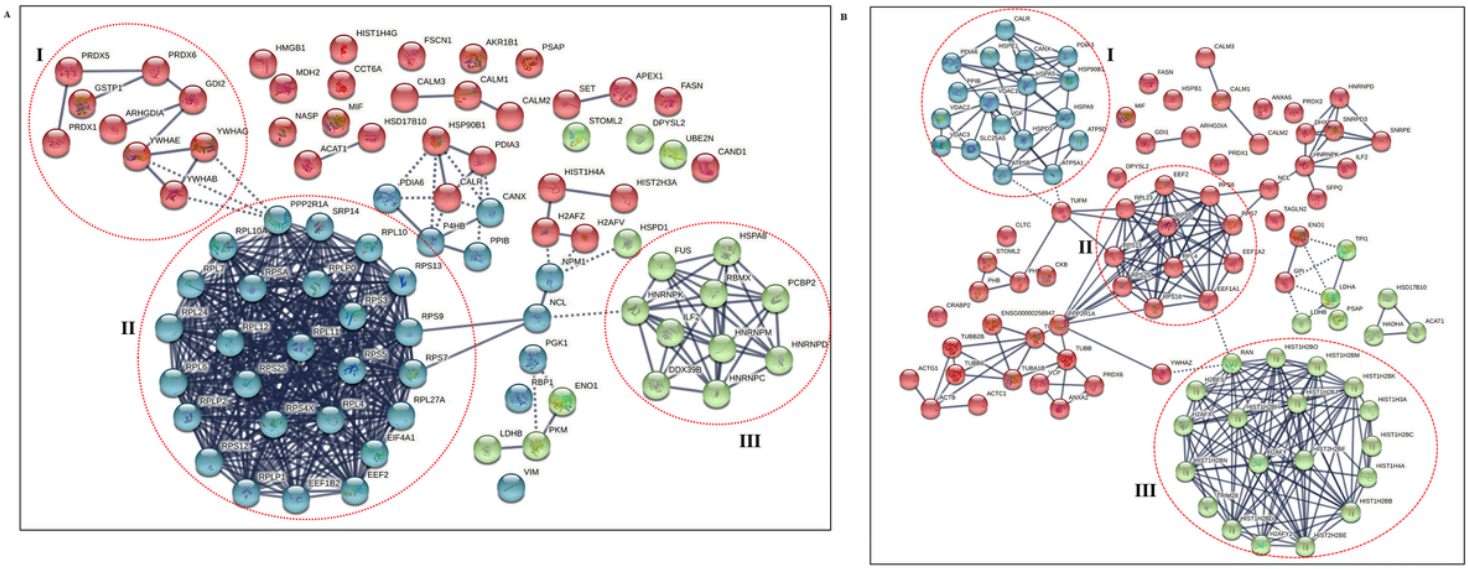

Figure 3

(A) STRING Protein-protein interaction network of differ-SH-SY5Y neural cells. The STRING PPI analysis of differentially regulated proteins in differ-SH-SY5Y neural cells vs undifferentiated SH-SY5Y cells. The red dotted circles show protein clusters with the highest confidence (0.9) interactions. The edges were drawn with different line thickness that indicates the strength of data support. (B) STRING Protein-protein interaction network of 6-OHDA induced neurodegeneration on differ-SH-SY5Y neural cells. The STRING PPI analysis of differentially regulated proteins in 6-OHDA treatment on differ-SH-SY5Y neural cells vs untreated differ-SH-SY5Y cells. The red dotted circles show protein clusters with the highest confidence (0.9) interactions. The edges were drawn with different line thickness that indicates the strength of data support.

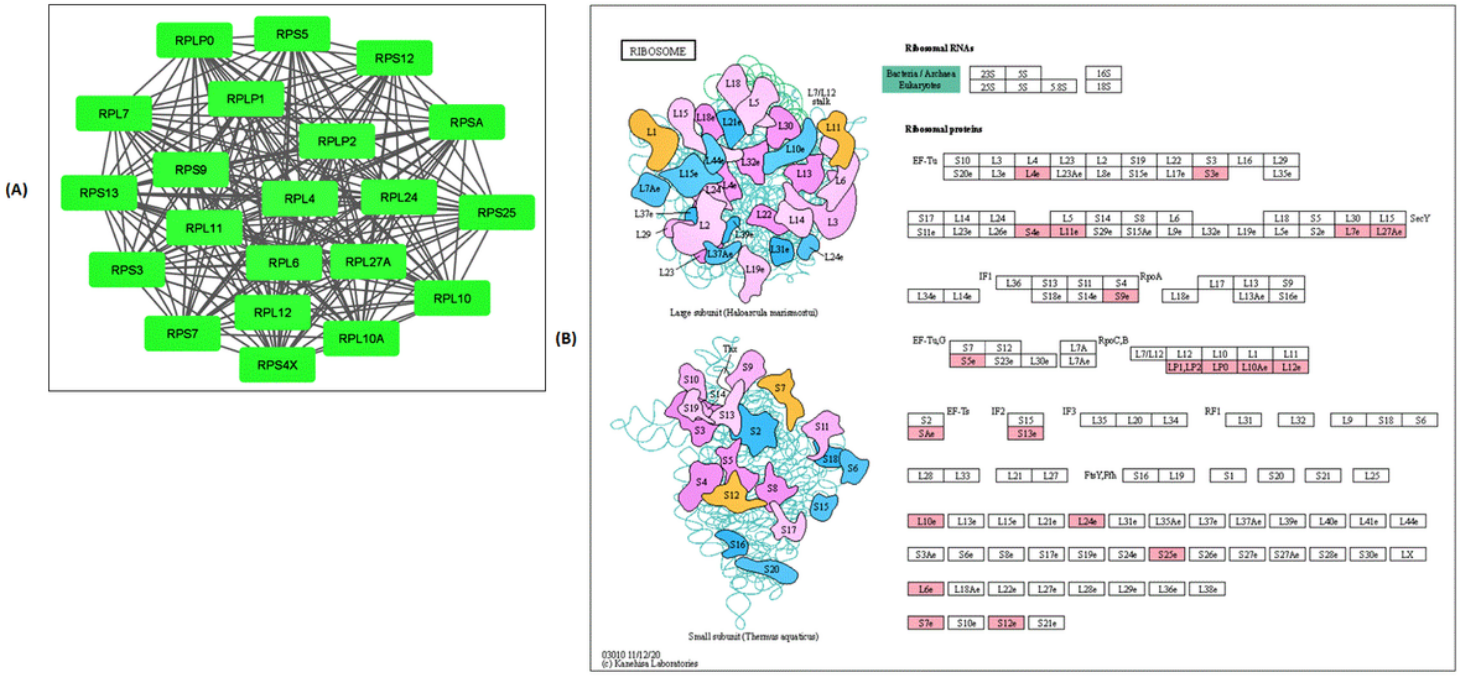

Figure 4

KEGG Pathway enrichment analysis of Cluster II proteins. (A) The differentially regulated cluster II protein network is visualized using Cytoscape 3.8.0. The green nodes indicate the significantly down-regulated cluster II proteins ($p<0.05$). (B) The position of cluster II proteins in the KEGG-ribosome pathway during the neuronal maturation in differ-SH-SY5Y neural cells are shown as pink-coloured boxes. The cluster II proteins involved in this pathway are ribosomal protein family members that can be classified as large subunit ribosomal proteins (RPL10, RPL10A, RPL11, RPL12, RPL24, RPL27A, RPL4, RPL6, RPL7, RPLP0, RPLP1, RPLP2) and small subunit ribosomal proteins (RPS12, RPS13 RPS25, RPS3, RPS4X, RPS5, RPS7, RPS9, RPSA) (Adapted from KEGG Ribosome pathway- ko03010).

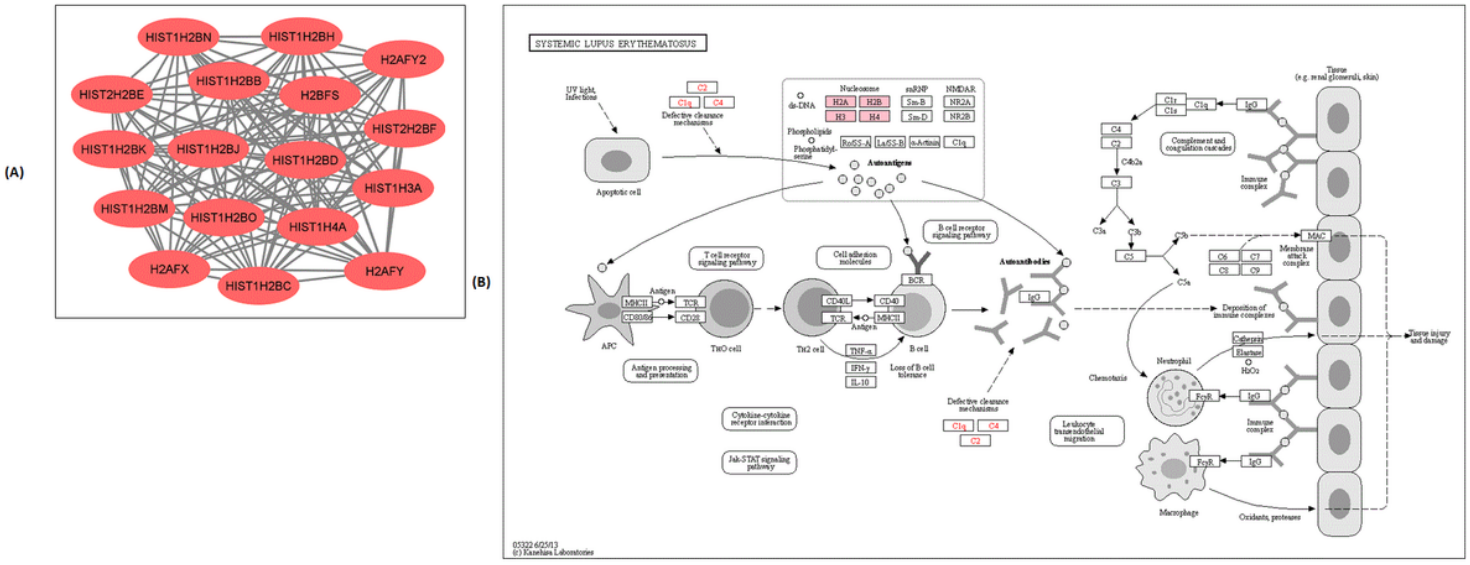

Figure 5

KEGG Pathway enrichment analysis of Cluster III proteins. (A) The differentially regulated cluster III protein network in differ-SH-SY5Y neural cells in response to 6-OHDA is visualized using Cytoscape 3.8.0. The Red nodes indicate the significantly upregulated cluster III proteins ($p<0.05$). (B) The position of cluster III proteins in the KEGG SLE pathway during the 6-OHDA induced neurodegeneration process are shown as pink-coloured boxes. The 17 cluster III proteins involved in this pathway are from H2A histone family member (H2AFX, H2AFY, H2AFY2), Histone H2B type (H2BFS), Histone cluster 1 H2B family (HIST1H2BB, HIST1H2BC, HIST1H2BD, HIST1H2BH, HIST1H2BJ, HIST1H2BK, HIST1H2BM, HIST1H2BN, HIST1H2BO), Histone cluster 1 H3 family (HIST1H3A), Histone cluster 1 H4 family (HIST1H4A) and Histone cluster 2 H2B family (HIST2H2BE, HIST2H2BF) (Adapted from KEGG Systemic Lupus Erythematosus pathway- hsa05322).

Supplementary Files

This is a list of supplementary files associated with this preprint. Click to download.

- Table1andTable2.pdf